JACS
JOURNAL OF THE AMERICAN CHEMICAL SOCIETY

COMMUNICATION

pubs.acs.org/JACS

The Amyloid Formation Mechanism in Human IAPP: Dimers Have β-Strand Monomer−Monomer Interfaces

Nicholas F. Dupuis, Chun Wu, Joan-Emma Shea, and Michael T. Bowers*

Department of Chemistry and Biochemistry, University of California Santa Barbara, Santa Barbara, California 93106, United States

Supporting Information

ABSTRACT: Early oligomerization of human IAPP (hIAPP) is responsible for β-cell death in the pancreas and is increasingly considered a primary pathological process linked to Type II Diabetes (T2D). Yet, the assembly mechanism remains poorly understood, largely due to the inability of conventional techniques to probe distributions or detailed structures of early oligomeric species. Here, we describe the first experimental data on the isolated and unmodified dimers of human (hIAPP) and nonamyloidogenic rat IAPP (rIAPP). The experiments reveal that the human IAPP dimers are more extended than those formed by rat IAPP and likely descend from extended monomers. Independent all-atom molecular dynamics simulations show that rIAPP forms compact helix and coil rich dimers, whereas hIAPP forms β-strand rich dimers that are generally more extended. Also, the simulations reveal that the monomer−monomer interfaces of the hIAPP dimers are dominated by β-strands and that β-strands can recruit coil or helix structured regions during the dimerization process. Our β-rich interface contrasts with an N-terminal helix-to-helix interface proposed in the literature but is consistent with existing experimental data on the self-interaction pattern of hIAPP, mutation effects, and inhibition effects of the N-methylation in the mutation region.

Protein aggregation and fibril formation are central processes in many age related diseases including Alzheimer's Disease, Parkinson's Disease, and Type II Diabetes (T2D).[1] In 1987, Islet Amyloid Polypeptide (hIAPP) was identified as the primary component of the amyloid deposits found in and around the β-cells in patients with T2D.[2] Although a structure of hIAPP fibrils has been obtained, structures of early oligomers and the mechanism of β-sheet formation remain poorly understood for this 37 residue peptide (KCNTATCATQ^{10}RLANFLV**H**SS^{20}NN**F**G**AIL**SS**T**^{30}NVGS-NTY-NH_2).[3] Further, early oligomers have been implicated as the primary cytotoxic components of the aggregation pathway.[4] Thus, characterizing the structures of early hIAPP oligomers is critical for a better understanding of the aggregation process.

In our previous study,[5] ion mobility spectrometry combined with mass spectrometry (IMS-MS) was used to characterize the size distribution of monomeric hIAPP and the nonamyloidogenic rat IAPP (KCNTATCATQ^{10}RLANFLV**R**SS^{20}NN**L**G**PV**L**PP**T^{30}NVGSN-TY-NH_2), which differs from hIAPP by only 6 amino acids mainly located between residues 20−29, called the "mutation region".[6,7] Experiments indicated hIAPP has an extended structural family not found in rIAPP.[5] By direct comparison with replica exchange molecular dynamics (MD) simulations, two experimental hIAPP conformer families were identified: a compact helix-coil family and an extended β-hairpin family, with the mutation region adopting coil and β-strand conformations respectively. In contrast to hIAPP, the simulations indicated that rIAPP only populates compact coil-rich and helix-coil families (with coiled mutation regions) in agreement with experiment.[5,8,9] Based on these results, a mechanism of hIAPP aggregation was proposed with direct side-by-side assembly of β-hairpin monomers to form β-sheet rich oligomers.[5] This "early conformation transition" mechanism highlights the conversion of monomers into β-sheet rich oligomers, which can be considered assembly prone structures.[5,9−11] This model contrasts with a paradigm of fibril formation where the N-terminal helix interactions drive assembly to form helix-rich oligomers, followed by a "phase transition", to β-sheet structured aggregates, later in the aggregation cascade.[12−15] Transient increases of helical content from NMR[14] and CD data[12] were used to infer the helix−helix assembly model. Yet, these techniques provide an average picture of peptide aggregation since neither method can distinguish oligomers from monomers. Also, by fusing a full length hIAPP to a 370-residue maltose binding protein (MBP), Eisenberg et al. were able to obtain a crystal structure of an hIAPP homodimer with residues 8−18 in helical conformations at the monomer−monomer interface.[16] However, this helix−helix interface may well be a result of crystal packing of the large fusion protein. This possibility is consistent with a lack of a helix−helix interface in the crystal of the second fusion protein (MBP fused with the N-terminal fragment (1−22) of hIAPP).[16]

Here, the combined IMS-MS and MD modeling approach[5] is used to investigate the structure of unmodified, isolated dimers of rIAPP and hIAPP. This study breaks new ground in amyloid formation mechanisms as currently there are no detailed experimental descriptions of dimer structure in the literature for amyloid systems with the complexity of hIAPP. The dimer is crucial as it provides the first, and best, opportunity to study the dynamics and structure of the monomer−monomer interface that drives further oligomer growth. This interface will be a focal point of this study and will provide insight into why hIAPP proceeds to form β-sheet fibrils and rIAPP does not. Also, it will shed light on the self-interaction pattern between 10-residue fragments of hIAPP and the full length hIAPP determined by fluorescence titration binding assays[17] and the working mechanism of the designed peptide inhibitors based on N-methylations in the mutation region.[18−20]

Sample preparation is discussed in supporting information(SI). All experiments were run on a home built nano-ESI IMS-MS

Received: September 15, 2010

   dx.doi.org/10.1021/ja1081537 | J. Am. Chem. Soc. XXXX, XXX, 000–000

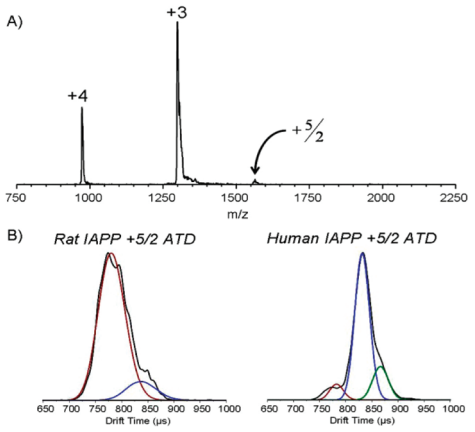

Figure 1. (A) Nano-ESI mass spectrum of hIAPP. (B) Rat and Human IAPP +5 dimer ATDs. Each ATD is fit with multiple features using the procedure described in the SI.

Table 1. Collision Cross Sections for Monomers and Dimers and the Relative Contributions of the Features in the +5/2 ATDs

	Monomer[a] δ (Å^2)	Dimer δ (Å^2)	Dimer % Contribution	Avg. BE[b] (kcal/mol)
Human IAPP	653	1024	7.4	−59.5
	770	1150	74.7	
		1225	17.9	
Rat IAPP	644	1033	87.8	−38.3
		1170	12.2	

[a] Reference 5. [b] The average dimer BEs from the simulations are included for each peptide.

instrument described previously.[21] Arrival time distributions (ATDs) of the z/n = +5/2 peaks of hIAPP and rIAPP are shown in Figure 1B. The ATDs were fit with multiple features, using the procedure described in the SI. Collision cross sections and relative abundances are listed in Table 1. The rIAPP ATD was best fit with two components. The compact species (1033 Å^2) comprises ∼88% of the ion intensity and is broader than expected for a single conformation, suggesting there may be multiple families contributing to this peak. The hIAPP ATD was best fit with three features. In this ATD the 1150 Å^2 peak is most abundant, contributing ∼75% of the ion intensity.

Comparison of the two most abundant features for each peptide shows that the hIAPP dimer is ∼12% larger in cross section than the rIAPP dimer (1033 Å^2 → 1150 Å^2). The larger hIAPP dimer cross section is consistent with the previous observation of hIAPP β-hairpin monomers that are ∼17% larger than the coil-rich rIAPP monomers.[5] The dimer cross sections can be estimated from monomers and should be larger by a factor of $2^{2/3}$, assuming no change in the monomer structure on forming the dimer.[21,22] From this approximation, dimers formed from compact hIAPP and rIAPP monomers are expected to have cross sections of ∼1030 Å^2 (650 Å^2 × $2^{2/3}$). Yet, dimers assembled from β-hairpin monomers are expected to have cross sections of ∼1220 Å^2 (770 Å^2 × $2^{2/3}$). This simple analysis suggests that some of the hIAPP dimers, with experimental cross sections of 1225 Å^2, may be directly assembled from β-hairpin-like monomers. The major dimer structural family, with a cross section of 1150 Å^2, also appears to have significant extended β-strand character. Overall, the extended conformations of the hIAPP monomers and dimers, compared with rIAPP, suggest that extended hIAPP conformations may play a critical role in the early stages of amyloid fibril formation and that β-strand character emerges early in the aggregation cascade.

Independent from the experiment, the hIAPP and rIAPP dimers were modeled with all-atom molecular dynamics simulations using the AMBER protein force field (ff96) coupled with a recent generalized Born implicit solvent (IGB = 5). Recent achievements of this ff96/IGB5 combination include the successful *ab initio* folding of α, β, and α/β proteins[23−26] and amyloid peptides including a prion fragment[27] and IAPP.[5] For all trajectories, the most populated monomer structural families identified in the previous study were used as the starting structures.[5] Full details of the modeling are included in the SI. The average binding energies (BEs) for each peptide are listed in Table 1, and the dimer structures, formed from monomers, are given in Figure 2. The mutation regions containing residues 22−29 of hIAPP and rIAPP are colored red to identify their role in the monomer−monomer interface.

The rIAPP results are given in Fig 2A. In all cases coil rich dimers are formed, often with reduced amounts of helix relative to the corresponding monomers. In contrast, the hIAPP results given in Fig 2B indicate all solution phase dimers have significant or dominant β-strand interfaces, one of which contains the mutation region. Our results for hIAPP are consistent with a recent literature calculation initiated from two hairpin monomers.[9] Of particular interest is trajectory H3 where N-terminal helices are converted to hairpin in the interface region.

The simulations here highlight four new insights about the assembly of both IAPP peptides. First, in all of the hIAPP dimers, the binding interface occurs almost exclusively between β-strand secondary structural segments containing the mutation region, rather than between the N-terminal helices. Additionally, side-by-side assembly between the β-hairpins is the major binding mode, whereas stacking between the β-hairpins is a more minor contributor. Interestingly, two strand regions of our hairpin structure (i.e., residues 11−18 and 23−32) in the monomer−monomer interface of H1 are coincident with the hot regions (i.e., residues 8−18 and 22−28) of the hIAPP−hIAPP interaction interface as determined by fluorescence titration binding assays.[17] Thus, independent measurements of the interaction interface support the results of our modeling. In contrast, rIAPP forms almost no β-strand and the dimers predominantly interact through the coil secondary structural segments. Together these simulations suggest that α-helix stacking is likely not a primary mode of peptide assembly.

Second, the simulations reveal the conversion of α-helix and coil secondary structures to β-strand during hIAPP dimerization. In the H3 trajectory (Figure 2B), an increase of β-strand from 16% to 33% was observed, with a corresponding decrease of α-helix from 27% to 13%. This recruitment effect was especially apparent in the +8 dimers; the coil structure (residue 19−37) of the helix-coil monomer was converted into β-strand in three separate trajectories. Again, the mutation region is located directly at the interface. This process is illustrated for a single trajectory in Figure 3.

Third, our side-by-side sheet assembly around the mutation region may explain the working mechanism of the N-methylated hIAPP in which two methyl groups were added to the amide nitrogens of G24 and I26 located within the mutation region causing a dramatic

dx.doi.org/10.1021/ja1081537 |*J. Am. Chem. Soc.* XXXX, XXX, 000–000

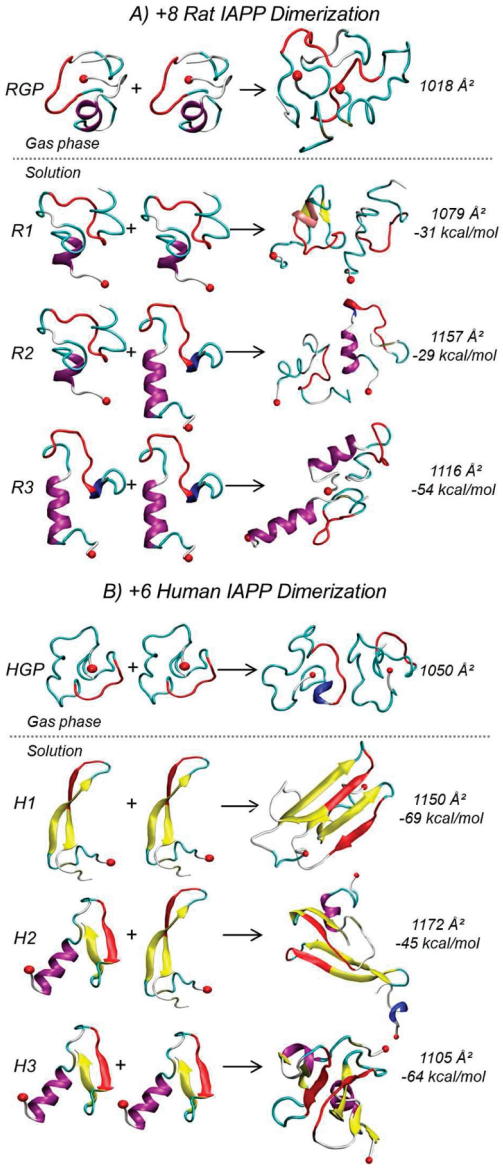

Figure 2. Representative dimerization trajectories of rIAPP (A) and hIAPP (B) in gas phase and solution. Residues 22−29 in the mutation region are colored in red.

reduction of amyloid fibril formation. N-methylation may prevent interstrand hydrogen bond formation and block the side-by-side sheet assembly. In a similar way, our model may explain the inhibition mechanism of the designed inhibitors containing NF(N-Me)GA (N-Me)IL.[19,20] One side of these inhibitors might bind to the native hIAPP and the other side with N-methylated groups preventing further side-by-side β-sheet formation.

Lastly, the simulations show that the hIAPP dimer BEs (−59.5 kcal/mol, Table 1) are, on average, larger than the rIAPP dimer BEs (−38.3 kcal/mol). The trend from our implicit solvent calculations is consistent with that from the potential of mean force calculations of dimer formation of hIAPP(20−29) and rIAPP(20−29) in explicit solvent.[28] The helix-helix model of association[16] yielded a BE of the helical dimer structure (PBD ID 3G7 V) of −26.2 kcal/mol, which is far less favorable than the −59.5 kcal/mol BE of β-strand bound hIAPP dimers. These calculations indicate that the β-strand, rather than the helix, motif

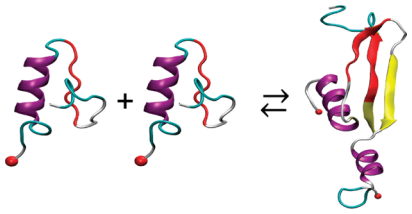

Figure 3. The hIAPP +8 (HH) trajectory shows conversion of coil into β-strand upon dimerization.

is generally a more stable and favorable interface for dimer formation and β-sheet nucleation than other secondary structures. This result is consistent with the observed differences in aggregation behavior of the two peptides.[29]

When comparing the experiments and simulations of the rIAPP peptide in this study, the gas phase dimer (RGP) and the compact coil-rich dimer (R1) are in closest agreement at 1.5% below and 4.5% above the experimental cross section of 1033 Å^2. Dimers from the other two trajectories (R2 and R3) may also make contributions to the experimental ATD as they fall within the limit of the largest experimental cross section (1170 Å^2). For the hIAPP peptide, the +6 dimers are considered because they are closest to the experimentally observed +5 charge state. Overall, all three trajectories with implicit solvent produced structures with cross sections (1105, 1150, and 1172 Å^2) that were in reasonably good agreement with the experimental value of 1150 Å^2. The gas phase dimer structure at 1050 Å^2 is also close to the most compact feature in the ATD at 1024 Å^2, which is very minor comprising only 7% of the total conformations observed experimentally. The simulations indicate that the hIAPP dimers are more energetically stable than the rIAPP dimers suggesting that the hIAPP dimers are more likely to retain more solution character during the experiment than rIAPP dimers.

In summary, experiments show hIAPP forms dimers that are significantly more extended than those formed by rIAPP, suggesting they have a high percentage of β-sheet content and may descend from β-hairpin monomers. The data are supported by models that reveal three routes to β-sheet formation in the dimers: (1) two β-hairpins associate side-by-side to form a four strand β-sheet (H1); (2) the hairpins stack, forming a two layer structure;[9] and (3) the α-helix or coil structures are recruited to form β-strands (H2 and H3). Furthermore, β-strands including the mutation region play a critical role in the monomer−monomer interface. In contrast, the rIAPP modeling shows compact and disordered dimers are formed from coil-rich structures with cross sections in good agreement with experiment.

Based on these results an updated assembly mechanism for hIAPP is shown in Figure 4. In this mechanism, the monomer can interconvert between a structure with an N-terminal helix and a β-hairpin structure. Simulations predict significant heterogeneity in the C-terminus of the α-helical monomer.[5] A β-strand rich dimer is now included in the aggregation pathway. Even though the hIAPP dimer may have multiple contributing conformers, the parallel side-by-side dimer is specifically included in the figure as it appears to have the greatest likelihood of propagating larger β-structured aggregates and fibrils. We note that further structural reorganization in forming multilayered β-structured aggregates is necessary to produce final mature fibrils such as that illustrated by Tycko's fibril model structure.[3] Overall, both the experiment and simulation results provide further support for a route to the fibril state through an "early

dx.doi.org/10.1021/ja1081537 |J. Am. Chem. Soc. XXXX, XXX, 000–000

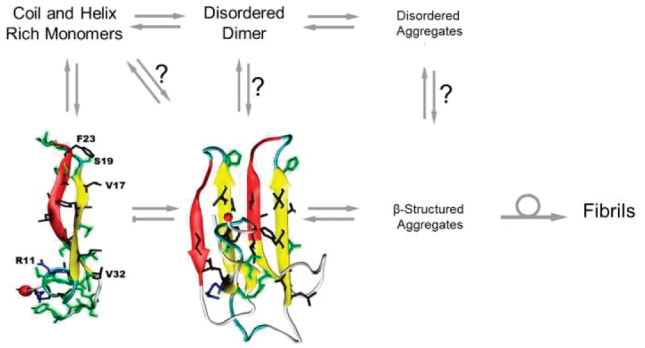

Figure 4. An updated proposed assembly mechanism for hIAPP is shown including a β-sheet rich dimer. This addition supports the β-structured aggregates rather than the disordered aggregates as "on" pathway species.

conformational transition" to a β-stranded conformer, a result that contrasts with the current "phase transition" paradigm via coiled or helix-rich oligomers for fibril formation in amyloid systems.

■ ASSOCIATED CONTENT

Supporting Information. Experimental details and mass spectra of rIAPP. Analysis of full MD simulation trajectories and dimer structures (PDB files are available upon request). This material is available free of charge via the Internet at http://pubs.acs.org.

■ AUTHOR INFORMATION

Corresponding Author
bowers@chem.ucsb.edu

■ ACKNOWLEDGMENT

Funding for this study was provided by the NIH, the NSF under grants CHE-0909743 (M.T.B.) and MCB-0642088 (J.E.S.), and the David and Lucile Packard Foundation (J.E.S.). The computer time was provided by Texas Advanced Computing Center (LRAC MCA 05S027). We are grateful to Dan Raleigh for supplying us with samples of hIAPP and rIAPP (funded by the NIH under Grant NIH-GM078114).

■ REFERENCES

(1) Sipe, J. D. *Amyloid proteins: the β-sheet conformation and disease*; Wiley-VCH: Weinheim, 2005.
(2) Westermark, P.; Wernstedt, C.; Wilander, E.; Hayden, D. W.; Obrien, T. D.; Johnson, K. H. *Proc. Natl. Acad. Sci. U.S.A.* **1987**, *84* (11), 3881–3885.
(3) Luca, S.; Yau, W. M.; Leapman, R.; Tycko, R. *Biochemistry* **2007**, *46* (47), 13505–13522.
(4) Lin, C. Y.; Gurlo, T.; Kayed, R.; Butler, A. E.; Haataja, L.; Glabe, C. G.; Butler, P. C. *Diabetes* **2007**, *56* (5), 1324–1332.
(5) Dupuis, N. F.; Wu, C.; Shea, J.-E.; Bowers, M. T. *J. Am. Chem. Soc.* **2009**, *131* (51), 18283–18292.
(6) Bernstein, S. L.; Dupuis, N. F.; Lazo, N. D.; Wyttenbach, T.; Condron, M. M.; Bitan, G.; Teplow, D. B.; Shea, J. E.; Ruotolo, B. T.; Robinson, C. V.; Bowers, M. T. *Nat. Chem.* **2009**, *1* (4), 326–331.
(7) Wyttenbach, T.; Bowers, M. T. *Top. Curr. Chem.* **2003**, *225*, 207–232.
(8) Reddy, A. S.; Wang, L.; Lin, Y. S.; Ling, Y.; Chopra, M.; Zanni, M. T.; Skinner, J. L.; De Pablo, J. J. *Biophys. J.* **2010**, *98* (3), 443–451.
(9) Reddy, A. S.; Wang, L.; Singh, S.; Ling, Y.; Buchanan, L.; Zanni, M. T.; Skinner, J. L.; De Pablo, J. J. *Biophys. J.* **2010**, *99* (7), 2208–2216.
(10) Kayed, R.; Bernhagen, J.; Greenfield, N.; Sweimeh, K.; Brunner, H.; Voelter, W.; Kapurniotu, A. *J. Mol. Biol.* **1999**, *287* (4), 781–796.
(11) Straub, J.; Thirumalai, D. *Curr. Opin. Struct. Biol.* **2010**, *20* (2), 187–195.
(12) Abedini, A.; Raleigh, D. *Phys. Biol.* **2009**, *6* (1), 015005.
(13) Chiti, F.; Dobson, C. M. *Annu. Rev. Biochem.* **2006**, *75*, 333–366.
(14) Williamson, J. A.; Miranker, A. D. *Protein Sci.* **2007**, *16* (1), 110–117.
(15) Wiltzius, J. J. W.; Sievers, S. A.; Sawaya, M. R.; Cascio, D.; Popov, D.; Riekel, C.; Eisenberg, D. *Protein Sci.* **2008**, *17* (9), 1467–1474.
(16) Wiltzius, J.; Sievers, S.; Sawaya, M.; Eisenberg, D. *Protein Sci.* **2009**, *18* (7), 1521–1530.
(17) Andreetto, E.; Yan, L.; Tatarek-Nossol, M.; Velkova, A.; Frank, R.; Kapurniotu, A. *Angew. Chem., Int. Ed.* **2010**, *49* (17), 3081–3085.
(18) Kapurniotu, A.; Schmauder, A.; Tenidis, K. *J. Mol. Biol.* **2002**, *315* (3), 339–350.
(19) Tatarek-Nossol, M.; Yan, L.; Schmauder, A.; Tenidis, K.; Westermark, G.; Kapurniotu, A. *Chem. Biol.* **2005**, *12* (7), 797–809.
(20) Yan, L. M.; Tatarek-Nossol, M.; Velkova, A.; Kazantzis, A.; Kapurniotu, A. *Proc. Natl. Acad. Sci. U.S.A.* **2006**, *103* (7), 2046–2051.
(21) Wyttenbach, T.; Kemper, P. R.; Bowers, M. T. *Int. J. Mass Spectrom.* **2001**, *212* (1−3), 13–23.
(22) Bleiholder, C.; Dupuis, N. F.; Wyttenbach, T.; Bowers, M. T. *Nat. Chem.* **2011**, *3* (2), 172.
(23) Shell, M. S.; Ritterson, R.; Dill, K. A. *J. Phys. Chem. B* **2008**, *112* (22), 6878–6886.
(24) Voelz, V.; Bowman, G.; Beauchamp, K.; Pande, V. *J. Am. Chem. Soc.* **2010**, *132* (5), 1526–1528.
(25) Voelz, V.; Singh, V.; Wedemeyer, W.; Lapidus, L.; Pande, V. *J. Am. Chem. Soc.* **2010**, *132* (13), 4702–4709.
(26) Wu, C.; Shea, J.-E. *PLoS Comput. Biol.* **2010**, *6* (11), e1000998.
(27) Grabenauer, M.; Bernstein, S. L.; Lee, J. C.; Wyttenbach, T.; Dupuis, N. F.; Gray, H. B.; Winkler, J. R.; Bowers, M. T. *J. Phys. Chem. B* **2008**, *112* (35), 11147–11154.
(28) Rivera, E.; Straub, J.; Thirumalai, D. *Biophys. J.* **2009**, *96* (11), 4552–4560.
(29) Goldsbury, C.; Goldie, K.; Pellaud, J.; Seelig, J.; Frey, P.; Muller, S. A.; Kistler, J.; Cooper, J. S.; Aebi, U. *J. Struct. Biol.* **2000**, *130* (2−3), 352–362.